Phase Winding a Two-Component Bose-Einstein Condensate in an Elongated Trap: Experimental Observation of Moving Magnetic Orders and Dark-Bright Solitons

C. Hamner, Yongping Zhang,* J. J. Chang, Chuanwei Zhang,† and P. Engels‡
Department of Physics and Astronomy, Washington State University, Pullman, Washington 99164, USA
(Received 25 June 2013; published 26 December 2013)

We investigate the phase winding dynamics of a harmonically trapped two-component BEC subject to inhomogeneous Rabi oscillations between two pseudospin components. While the single-particle dynamics can be explained by mapping the system to a two-component Bose-Hubbard model, nonlinearities due to the interatomic repulsion lead to new effects observed in the experiments: In the presence of a linear magnetic field gradient, a qualitatively stable moving magnetic order that is similar to antiferromagnetic order is observed after critical winding is achieved. We also demonstrate how the phase winding can be used to generate copious dark-bright solitons in a two-component BEC, opening the door for new experimental studies of these nonlinear features.

DOI: 10.1103/PhysRevLett.111.264101 PACS numbers: 05.45.Yv, 03.75.Kk, 03.75.Lm, 03.75.Mn

Ferromagnetic (FM) and antiferromagnetic (AFM) orders are two important and fundamental linear magnetic orders in material physics. It is well known that AFM order exists in the underdoped and low temperature region of the phase diagram for high temperature cuprate superconductors [1]. Ultracold atoms provide a highly controllable experimental platform for emulating condensed matter phenomena. AFM order has been predicted to exist in quantum gases confined in optical lattices, but reaching the required low temperatures is very difficult [2,3]. Two-component BECs contain rich physics and have been investigated extensively in the past decade in both experiment and theory [4–9]. For a continuous two-component BEC in a harmonic trap, an AFM order can be defined similarly to that in lattices. Each spin component contains periodic and spatially well separated parts, and different spin components appear alternating in space.

In this Letter, we investigate the dynamics of an elongated two-component BEC subject to a spatially varying Rabi coupling between the two components. We show that the dynamics can lead to a phase resembling AFM order. The strong nonlinear interactions in the BEC play a key role. Without them, periodic winding and unwinding cycles analogous to the ones of [10,11] are observed instead. We present a mapping to a Bose-Hubbard model that explains these regular cycles. For the nonlinear case, our experiment and numerics show a succession of stages: A period of regular winding is followed by the emergence of an AFM-like pattern. Under the right conditions, the AFM ordering is accompanied by the appearance of a dressed state. We also demonstrate how such Rabi windings can be employed to generate trains of dark-bright (DB) solitons.

To showcase the winding dynamics, we start with a BEC containing about 450 000 ^{87}Rb atoms in the $|F, m_F\rangle = |1, -1\rangle$ hyperfine state. The condensate is confined in an effectively one-dimensional geometry formed by a 1064 nm single beam optical dipole trap with measured trap frequencies of $\{\omega_x, \omega_y, \omega_z\} = 2\pi \times \{178, 145, 1.5\}$ Hz. The atoms are coupled to the $|2, 0\rangle$ state via a microwave pulse of duration t. The scattering lengths are $a_{\uparrow\uparrow} = 100.4a_B$, $a_{\downarrow\downarrow} = 94.57a_B$, and $a_{\uparrow\downarrow} = 98.13a_B$ [12], where a_B is the Bohr radius. The choice of the $|1, -1\rangle$ and $|2, 0\rangle$ state produces a weakly immiscible system as determined from the mean field condition, $a_{\uparrow\downarrow}^2 > a_{\downarrow\downarrow}a_{\uparrow\uparrow}$ [13], but similar dynamics are observed for weakly miscible states as well [14]. The strength of the coupling pulse is characterized by the Rabi frequency Ω_0 which we measure to be 7.4 kHz, when on resonance. The atoms are placed in a magnetic field that consists of a 1 G field in the vertical (y) direction and a magnetic gradient field along the axial (z) direction, yielding a z gradient of about 0.017 G/cm. The gradient provides the means by which the detuning δ, and hence the local Rabi frequency Ω, vary across the cloud [15]. In our experiments, unless noted otherwise, the detuning at the center of the BEC is 1.3 kHz and the point of zero detuning is located to the left of the BEC in the images. The local Rabi frequency $\Omega_{\text{eff}} = \sqrt{\Omega_0^2 + \Delta^2}$ increases across the BEC from left to right. For imaging we use a spin selective technique described in [16]. It involves a short expansion period during which no Rabi drive is applied. Prior to the imaging, the two states are vertically overlapped.

While the microwave coupling is applied, windings develop that move in space with a fixed speed set by the local Rabi frequency [17]. The windings move out of the BEC at one end while new windings emerge at the other end. In Fig. 1(a), a short coupling pulse lasting $t = 10$ ms creates only two windings across the cloud. Longer coupling pulses result in more windings with very regular spacing along the axial direction [Figs. 1(b) and 1(c)]. Interestingly, for the chosen parameters this increase in the number of windings

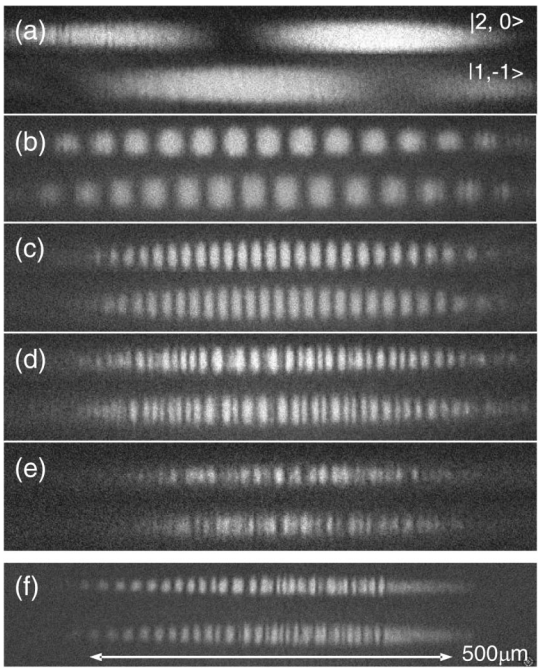

FIG. 1. Phase winding with a detuning gradient across the axial extent of the BEC. The $|2,0\rangle$ state (top cloud in each panel) is coupled to the $|1,-1\rangle$ (bottom cloud) via a microwave pulse of duration (a) 10 ms, (b) 100 ms, (c) 200 ms, (d) 300 ms, and (e) 900 ms. (f) Image taken at larger Raman detuning, but similar gradient, and a winding duration of 600 ms.

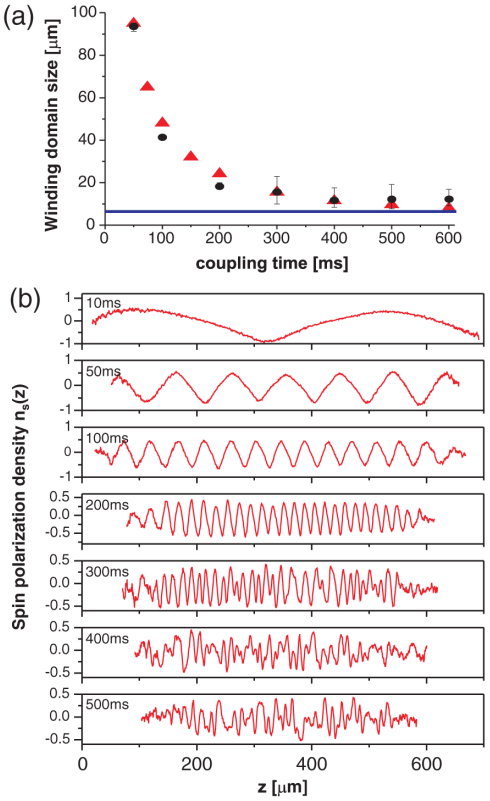

FIG. 2 (color online). (a) Saturation of the spatial spin polarization. The domain size, measured in the central region of the BEC, stops decreasing after $t \approx 300$ ms. Overlaid with the experimental results (black circles), where the error bar indicates the variation in the domain size across the central region of the BEC, are numerical results (red triangles). The horizontal line (blue) indicates twice the spin healing length for the initial atom number of the BEC. (b) Radially integrated spin polarization for the winding durations indicated in each panel.

ceases when the winding duration reaches $t \approx 300$ ms, corresponding to an average experimentally observed domain spacing of 15 μm and central domain spacing of 8 μm [Fig. 1(d)]. Following this duration the pattern remains qualitatively unchanged for several hundred ms, in the sense that experimental images taken during this interval show domains of similar size, albeit the exact positions of the detected domains vary from shot to shot. This long-time behavior is in stark contrast to the behavior observed in less elongated trapping geometries in which the condensate winds and unwinds [10,11]. After several hundred ms, atom number losses, particularly for the $|2,0\rangle$ state, become significant.

To characterize the formation of the magnetic order, we plot the minimum domain size of each spin component versus the coupling time in Fig. 2(a). We see that the experimental domain size decreases and then saturates after $t \approx 300$ ms. The solid (blue) horizontal line indicates $2\zeta_{\mathrm{spin}}$ for the initial atom number and central density. For these experimental parameters, the magnetic order becomes qualitatively fixed when the domain size approaches twice the spin healing length $\zeta_{\mathrm{spin}} = 1/\sqrt{8\pi n|a|}$, where n is the local density, $a = (2a_{\downarrow\uparrow} - a_{\downarrow\downarrow} - a_{\uparrow\uparrow})/2$, and $a_{\alpha\beta}$ are the s-wave scattering lengths [18].

In Fig. 2(b), we plot the experimentally observed radially integrated spin polarization density $n_s(z) = [n_\uparrow(z) - n_\downarrow(z)]/[n_\uparrow(z) + n_\downarrow(z)]$ after several different winding durations. The emergence of a magnetic order similar to the AFM state, after the Rabi winding saturates, is clearly evidenced by the periodic variation of the spin polarization density in this system. However, $n_s(z)$ does not reach unity after a long time (i.e., the density of one spin component does not fully disappear). We attribute this to the large kinetic energy needed for the complete disappearance of one spin component, to the finite resolution of the imaging system, or to possible expansion dynamics during the TOF imaging. Note that in contrast to AFM orders in optical lattices where AFM ground states require ultralow temperature and entropy, the moving AFM orders observed here are induced by the strong external Rabi coupling, and the temperature of the BEC plays a negligible role in such dynamics.

For experimental parameters where the spatial dependence of the winding rate is increased, a peculiar and qualitatively different behavior can be observed: In this case, our experimental as well as numerical studies reveal that extended parts of the BEC can enter a dressed state characterized by the absence of any winding dynamics in both

pseudospin components [19]. An example is shown in Fig. 1(f) where a larger winding rate is produced by using a similar magnetic gradient as before but a larger detuning of 4 kHz. After a coupling time of 600 ms the left edge of the BEC still exhibits Rabi winding while the right edge has evolved into a dressed state. The two regions are separated by the qualitatively stable AFM ordering.

The observed dynamics are well reproduced by numerical simulations using the one-dimensional Gross-Pitaevskii (GP) equation. Choosing the units of energy, time, and length of the system as $\hbar\omega_z$, ω_z^{-1}, and $\sqrt{\hbar/m\omega_z}$, we can write the coupled dimensionless equations as

$$i\frac{\partial}{\partial t}\begin{pmatrix}\Phi_\uparrow\\ \Phi_\downarrow\end{pmatrix}=\begin{pmatrix}H_\uparrow+\Delta(z) & \Omega_0\\ \Omega_0 & H_\downarrow\end{pmatrix}\begin{pmatrix}\Phi_\uparrow\\ \Phi_\downarrow\end{pmatrix}. \quad (1)$$

Here, $\Phi_\uparrow$ and $\Phi_\downarrow$ represent condensate wave functions in the hyperfine states $|1,-1\rangle$ and $|2,0\rangle$, respectively. $H_\uparrow = H_0 + 2N\sqrt{m\omega_x\omega_y/\hbar\omega_z}(a_{\uparrow\uparrow}|\Phi_\uparrow|^2 + a_{\uparrow\downarrow}|\Phi_\downarrow|^2)$ and $H_\downarrow = H_0 + 2N\sqrt{m\omega_x\omega_y/\hbar\omega_z}(a_{\downarrow\downarrow}|\Phi_\downarrow|^2 + a_{\uparrow\downarrow}|\Phi_\uparrow|^2)$, where $H_0 = -(\partial^2/2\partial z^2) + (z^2/2)$ and the second terms describe the mean field nonlinear interaction between atoms. N is the total atom number. $\Delta(z) = \Delta_0 + \delta z$ includes a constant detuning Δ_0 and the detuning δz caused by the magnetic gradient. We numerically solve the GP equation (1) using the experimental parameters as in Figs. 1(a)–1(e) and 2(a), and determine the domain spacing after various durations of the microwave pulse [red triangles in Fig. 2(a)]. We find good agreement between the numerical results and the experimental data. Our numerical simulations also reveal that the spin density polarization $n_s(z)$ does not reach unity after a long duration in the AFM phase, corroborating the experimental observation.

To emphasize the importance of the nonlinear interactions for these dynamics, we contrast the observed behavior with the predictions of a single-particle picture which ignores mean field contributions to the spin dynamics. In this case, regular winding and unwinding processes exist which can be understood from an insightful mapping to a two-component Bose-Hubbard model. We start from the linear system of Eq. (1) by neglecting nonlinear terms and expand $\Phi_\uparrow$ and $\Phi_\downarrow$ using the harmonic oscillator basis Ψ_j, $\Phi_\uparrow(z) = \sum_j a_j\Psi_j(z)$ and $\Phi_\downarrow(z) = \sum_j b_j\Psi_j(z)$. Substituting these expansions into Eq. (1), we obtain

$$\begin{aligned} i\frac{\partial a_j}{\partial t} &= \frac{1}{2}ja_j + \Omega_0 b_j + \Delta_0 a_j + \delta\sqrt{\frac{j+1}{2}}a_{j+1} \\ &\quad + \delta\sqrt{\frac{j}{2}}a_{j-1}, \\ i\frac{\partial b_j}{\partial t} &= \frac{1}{2}jb_j + \Omega_0 a_j, \end{aligned} \quad (2)$$

which is reminiscent of a two-component Bose-Hubbard model. This model can be interpreted as a lattice system subject to a linear potential $(1/2)z$, leading to the on-site energy $j/2$. The linear potential prevents the atom from climbing to large j. On the other hand, the effective tunneling coefficient is anisotropic: it is $\delta\sqrt{(j+1)/2}$ for $j \to j+1$, but $\delta\sqrt{j/2}$ for $j \to j-1$. Therefore, the atoms prefer to tunnel to large j sites. The competition between the linear potential and the anisotropic tunneling leads to a maximum j_0. Numerical simulations of Eq. (2) confirm that there exists a maximally occupied j for the dynamical oscillation of a_j and b_j with the initial condition $a_0 = 1$ and $b_0 = 0$. The jth harmonic oscillator wave function has j nodes, yielding $j+1$ possible domains in the density of each component. The largest maximally occupied mode during the single-particle winding is plotted in Fig. 3(a) for various axial confinements. This maximal winding number increases as the axial trap frequency ω_z is decreased while the magnetic gradient is kept fixed.

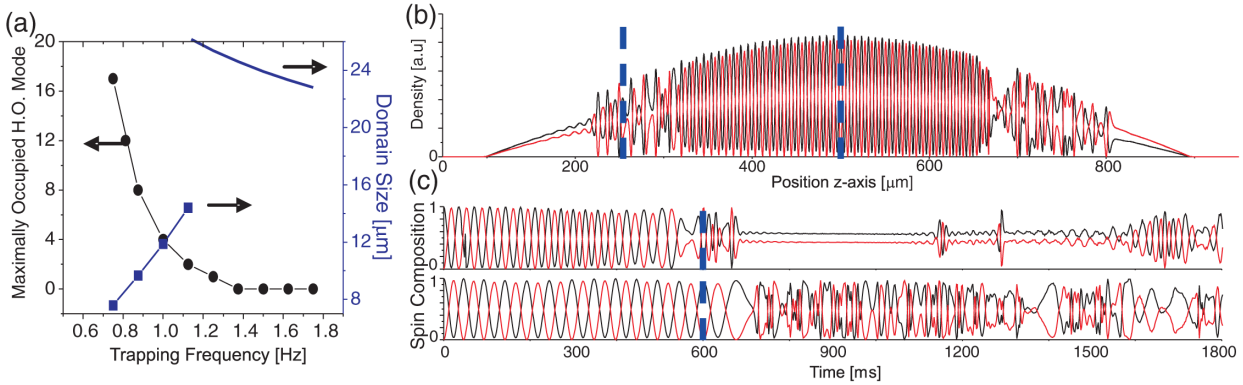

FIG. 3 (color online). (a) Effect of the axial confinement on the maximally wound single-particle system in the Bose-Hubbard model (black circles). The spin domain size for these maximal windings (blue squares) and twice the harmonic oscillator (HO) length (blue solid line) are overlaid. (b),(c) Numerical results of the 1D GP equation for experimental parameters. (b) Density distribution for the two spin states after 600 ms of the applied microwave coupling. (c) Temporal evolution of the spin populations at $z = 250$ μm (upper panel) and $z = 500$ μm (lower panel). In this graph the chosen 2 ms time steps lead to aliasing of the fast and regular Rabi cycles.

The addition of nonlinearity leads to the coupling of atoms to sites with higher j. This is expected based on the following. First, the repulsive interactions lead to a larger spatial extent of the BEC so that larger modes have to be occupied to reach the same domain spacing. Second, larger interactions reduce ζ_{spin}, decreasing the minimum possible domain size. The winding dynamics depart from the single-particle like recursions when the system attempts to flip its order parameter, to begin unwinding. Figures 3(b) and 3(c) show results of the 1D GP simulation for the experimental parameters. Figure 3(b) shows the density profile along the z axis after 600 ms winding, i.e., just before the winding fully saturates. Figure 3(c) shows time evolution plots for the local spin composition at the spatial locations indicated by the vertical lines in Fig. 3(b). The deviations from the single-particle like winding occur at different evolution times across the spatial extent of the BEC. The dynamics across the extent of the BEC no longer appear synchronized, leading to the AFM-like ordering. We note that, in the limit of small nonlinearity or large ω_z, the numerics recover the winding and unwinding behavior.

The phase winding can also be exploited as a tool to generate copious dark-bright solitons, enabling studies of their dynamics. During the phase winding, the quantum-mechanical phase advances by π between consecutive domains of the same component (neglecting a minor deviation from π induced by the finite and spatially varying detuning of the Rabi drive). This is a natural starting point for the generation of dark-bright solitons in which a dark soliton, with a phase jump of π, in one component is filled by a bright soliton in the second component [20]. As we experimentally demonstrate, the phase winding pattern can be transformed into a dark-bright soliton train. For the data shown in Fig. 4, we start by reproducing the situation in Fig. 1(c) and then abruptly turn off the applied gradient as well as the Rabi drive. The subsequent in-trap evolution is strongly influenced by the difference in lifetime between the $|1,-1\rangle$ and $|2,0\rangle$ states (30 sec versus 0.5 sec, respectively). As atoms are preferentially lost from the $|2,0\rangle$ state, the domains of the $|1,-1\rangle$ state approach each other. Assisted by the phase difference between domains in the $|1,-1\rangle$ state, dark solitons filled by atoms of the $|2,0\rangle$ state form. Figures 4(b)–4(d) show the evolution of these DB solitons. The consistent width and long lifetime of these structures provide evidence for their solitonic character as seen under other experimental conditions [16,21,22]. Though many DB solitons are formed that are initially equally spaced, the regularity of the arrangement is lost after longer wait times. A similar evolution of the wound BEC into solitons can also be observed for the longer-lived states $|1,-1\rangle$ and $|2,-2\rangle$, as seen in Fig. 4(e) with a 60 ms evolution time after the end of the Rabi drive. Here, DB solitons form with alternating polarity in both spin components at the interfaces between the spin domains. To our knowledge, this constitutes the first generation of a train of alternatingly polarized DB solitons in a BEC. This technique of generating copious solitons offers exciting prospects for the investigation of soliton gases [23,24] or complex soliton interactions, e.g., in "soliton molecules" [25].

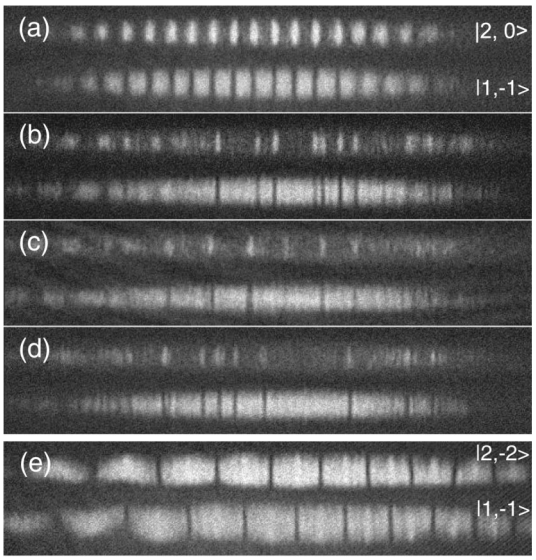

FIG. 4. Generation of dark-bright solitons via phase winding. After applying a coupling pulse of $t = 200$ ms, the magnetic gradient and coupling are jumped off and the clouds are allowed to evolve in trap for (a) 100 ms, (b) 300 ms, (c) 400 ms, and (d) 500 ms before imaging. (e) A BEC of atoms in the $|1,-1\rangle$ and $|2,-2\rangle$ state is wound and let evolve for 60 ms. Here, a DB soliton train with alternating polarity is generated.

C. H., J. J. C., and P. E. acknowledge financial support from NSF and ARO. Y. Z. and C. Z. acknowledge support from ARO (Grant No. W911NF-12-1-0334), AFOSR (Grant No. FA9550-11-1-0313), and NSF-PHY (No. 1249293). C. H., Y. Z., and J. J. C. contributed equally to this work.

*Present address: Quantum Systems Unit, Okinawa Institute of Science and Technology, Okinawa 904-0495, Japan.
†Present address: Department of Physics, University of Texas at Dallas, Richardson, TX 75080, USA. chuanwei.zhang@utdallas.edu
‡engels@wsu.edu

[1] P. A. Lee, N. Nagaosa, and X.-G. Wen, Rev. Mod. Phys. **78**, 17 (2006).
[2] C. J. M. Mathy, D. A. Huse, and R. G. Hulet, Phys. Rev. A **86**, 023606(R) (2012).
[3] D. Greif, T. Uehlinger, G. Jotzu, L. Tarruell, and T. Esslinger, Science **340**, 1307 (2013).
[4] See, e.g., M. Abad and A. Recati, Eur. Phys. J. D **67**, 148 (2013); B. J. Dalton and S. Ghanbari, J. Mod. Opt. **59**, 287 (2012), and references therein.
[5] J. Williams, R. Walser, J. Cooper, E. Cornell, and M. Holland, Phys. Rev. A **59**, R31 (1999).

[6] P. Öhberg and S. Stenholm, Phys. Rev. A **59**, 3890 (1999).
[7] D. S. Hall, M. R. Matthews, J. R. Ensher, C. E. Wieman, and E. A. Cornell, Phys. Rev. Lett. **81**, 1539 (1998).
[8] K. Sasaki, N. Suzuki, and H. Saito, Phys. Rev. A **83**, 033602 (2011).
[9] M. A. Hoefer, J. J. Chang, C. Hamner, and P. Engels, Phys. Rev. A **84**, 041605 (2011).
[10] M. R. Matthews, B. P. Anderson, P. C. Haljan, D. S. Hall, M. J. Holland, J. E. Williams, C. E. Wieman, and E. A. Cornell, Phys. Rev. Lett. **83**, 3358 (1999).
[11] J. Williams, R. Walser, J. Cooper, E. A. Cornell, and M. Holland, Phys. Rev. A **61**, 033612 (2000).
[12] S. J. J. M. F. Kokkelmans (private communication).
[13] E. Timmermans, Phys. Rev. Lett. **81**, 5718 (1998).
[14] We have experimentally observed similar winding dynamics and soliton generation in the longer-lived states $|1,-1\rangle$ and $|2,-2\rangle$ which are weakly miscible with scattering length $a_{\downarrow\downarrow} = 100.4a_0$, $a_{\uparrow\uparrow} = 98.98a_0$, and $a_{\downarrow\uparrow} = 98.98a_0$.
[15] In ^{87}Rb, the linear Zeeman effect leads to a shift of approximately 700 kHz/G of the $|1,-1\rangle$ state, while the $|2,0\rangle$ state remains unaffected (to first order). The variation of the detuning across the BEC also leads to a variation of the amplitude of the Rabi oscillation, which, however, is negligible for the chosen parameters.
[16] C. Hamner, J. J. Chang, P. Engels, and M. A. Hoefer, Phys. Rev. Lett. **106**, 065302 (2011).
[17] A. B. Deb, B. J. Sawyer, and N. Kjærgaard, Phys. Rev. A **88**, 063607 (2013).
[18] For our initial atom number the spin healing length at the BEC center is approximately 3.2 μm.
[19] P. B. Blakie, R. J. Ballagh, and C. W. Gardiner, J. Opt. B **1**, 378 (1999).
[20] B. P. Anderson, P. C. Haljan, C. A. Regal, D. L. Feder, L. A. Collins, C. W. Clark, and E. A. Cornell, Phys. Rev. Lett. **86**, 2926 (2001).
[21] C. Becker, S. Stellmer, P. Soltan-Panahi, S. Dörscher, M. Baumert, E. Richter, J. Kronjäger, K. Bongs, and K. Sengstock, Nat. Phys. **4**, 496 (2008).
[22] S. Middelkamp, J. J. Chang, C. Hamner, R. Carretero-González, P. G. Kevrekidis, V. Achilleos, D. J. Frantzeskakis, P. Schmelcher, and P. Engels, Phys. Lett. A **375**, 642 (2011).
[23] G. A. El and A. M. Kamchatnov, Phys. Rev. Lett. **95**, 204101 (2005).
[24] G. A. El, A. M. Kamchatnov, M. V. Pavlov, and S. A. Zykov, J. Nonlinear Sci. **21**, 151 (2011).
[25] D. Yan, J. J. Chang, C. Hamner, P. G. Kevrekidis, P. Engels, V. Achilleos, D. J. Frantzeskakis, R. Carretero-González, and P. Schmelcher, Phys. Rev. A **84**, 053630 (2011).